

## Design and development of modified high efficient high gain DC-DC converter for SPV standalone systems

Vineeth Kumar Pothera Kariyat, Jijesh Jisha Janardhanan

Department of Electronics and Communication, Sri Venkateshwara College of Engineering, Bangalore, India

### Article Info

#### Article history:

Received Nov 11, 2022

Revised Jan 13, 2023

Accepted Feb 6, 2023

#### Keywords:

DC-DC converter

Efficiency

HEHG converter

Solar photovoltaic applications

Voltage gain

### ABSTRACT

A conventional DC-DC converter is not viable for power conditioning in standalone solar photovoltaic applications. Switching losses are the primary reason for the poor performance of conventional DC-DC converters. To mitigate the issues in conventional DC-DC converters, a high efficient high gain (HEHG) DC-DC converter is designed and developed in this research work. Modified HEHG converter utilizes the passive components switched capacitors, coupled inductor, and resistor capacitor (RC) snubber circuit for minimizing the switching losses and improving the overall power conversion efficiency of the solar photovoltaic (SPV) system. In addition, a modified D-sweep maximum power point tracking (MPPT) algorithm is incorporated into this system to improve the tracking efficiency of the SPV system. HEHG for a standalone system is designed using MATLAB/Simulink environment and developed the hard-ware prototype. As a part of the validation, real-time testing is carried out and compares the performance of the HEHG converter with a traditional DC-DC converter. The theoretical efficiency of the HEHG converter is 96.01%, and the real-time efficiency is 95.62%. Found that theoretical and practical values of performance parameters are closely tallying.

This is an open access article under the [CC BY-SA](#) license.



### Corresponding Author:

Vineeth Kumar Pothera Kariyat

Department of Electronics and Communication Engineering, Sri Venkateshwara College of Engineering  
Bangalore, Karnataka 562157, India

Email: vineethkumarpk@gmail.com

## 1. INTRODUCTION

The energy crisis is one of the challenges faced by the global community. Conventional sources are diminishing as the energy demand is tremendously higher. The parallel world is facing global warming, pollution, and climate change. Therefore, it is essential to change the power generation from conventional to non-conventional sources systematically. Solar energy is more convenient than other renewable energy sources by considering the features such as modularity, installation, adaptability, and cost. When it comes to solar photovoltaic systems (SPV) performance entirely depends on the weather. In general, the solar panel output voltage is comparatively low. The panel voltage, such as the solar water pump, is insufficient to operate the standalone load. A conventional DC-DC boost converter is needed to step up the voltage from a lower to a higher level to meet the rated voltage of the load. Nevertheless, conventional DC-DC converter fails to step up the voltage from a lower level to a higher level because of a reduction in efficiency. The main reason for the reduction of the DC-DC converter is due to switching losses. Therefore, the conventional DC-DC converter is obsolete where the application requires high gain. To overcome this issue, an improved DC-DC converter is essential in the SPV system.

A modified DC-DC converter's salient features should have high gain without losing efficiency. There are plenty of topologies available in various literature. The principal reduction in the converter

efficiency is the self-heating of components, variation of current and voltage in the power converter [1], and wrong selection of heat sinks. The LLC-based resonant converter is an optimal choice for high voltage high gain applications, but the converter consists of a transformer that leads to transformer losses [2]. In addition to this setback, the cost of the LLC converter is more. The modified Cuk converter is another choice of high-gain application, but the inverted output restricted the widespread usage of the Cuk converter. Combined Luo converter with flyback topology helps to achieve high gain without losing efficiency. However, the SiC MOSFET switch used in the hybrid luo-flyback converter is expensive and not applicable to all situations. Significant research and development are required for cost reduction for the luo-flyback combination. Using a transformer in the hybrid luo-flyback converter does not make this converter more viable in all circumstances. The problem with a high step-up DC-DC converter is the requirement for large inductors and auxiliary circuits [3]. The improved SEPIC converter has the problem of a large inrush current in the inductor, high peak time, and high settling time value [4]. The quadratic boost converter (QBC) performs high voltage gain with a reduced duty cycle, But the voltage stress at the power switch is exceptionally high. QBC with a voltage double circuit is another convenient option, but the count of passive components increases the overall system size. Interleaved converters are also a convenient option for high voltage, high gain applications. Nevertheless, a voltage multiplier cell (VMC) with interleaved boost converter is needed to optimize high gain with high efficiency. However, the VMC increases system size and overall cost. Non-isolated coupled inductor topologies are a convenient option to perform high gain without compromising overall efficiency. The isolated converters [5], such as half-bridge converters, full-bridge converters, forward converters, and push-pull converters, are suitable options for high voltage high gain applications, but the transformer cost is not viable. Multilevel boost converter (MBC) can produce high gain, but it fails to produce actual output voltage corresponding to the duty cycle [6]. A proposed switched capacitor converter is another choice of high voltage high gain application, but eight power switches are used in this topology [6]. As the number of switches increases, the system becomes bulkier and more expensive. The proposed high efficient high gain converter (HEHG) topology utilized coupled inductor and switched capacitor that helps to minimize switching losses and EMI issues. Also, it helps to maintain high gains without losing system efficiency overcome the setbacks of conventional DC-DC converters. This research article is segmented into the following sections. Section 2 describes the research method; section 3 explains the results and discussion; and section 4 concludes the paper.

## 2. RESEARCH METHOD

The overall system comprises a solar photovoltaic panel, a HEHG converter, and a lamp load. In this system, the design and development of the HEHG converter is a novel concept. The components of the system are described below:

### 2.1. Mathematical modeling of solar photovoltaic panel

A solar photovoltaic cell is a transducer that converts light energy into electricity. It works on the principle of the photovoltaic effect. Different modeling methods are available for the modeling of PV panels, like single-diode modeling and two-diode modeling [7]. Single-diode modeling of PV cells is represented in Figure 1. PV cell is considered a current source.

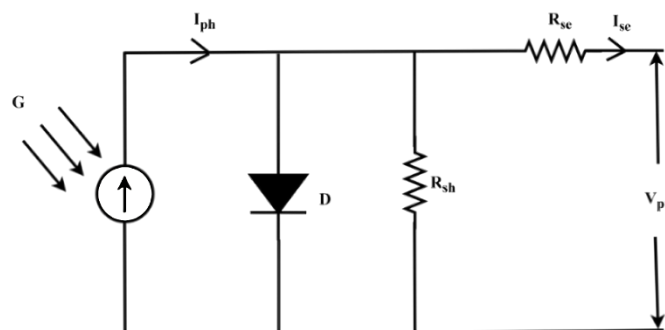


Figure 1. Single diode modeling of PV cell

The characteristics of PV cells are non-linear. The parameters of the PV cell are described below: current from the PV cell ( $I_{ph}$ ) is calculated using Kirchhoff's current law shown in (1).

$$I_{PV} = I_{ph} - I_d - I_{sh} \quad (1)$$

Where  $I_{pv}$  is the output current of the PV cell,  $I_{ph}$  is the photocurrent generated by a solar cell,  $I_d$  is the diode forward current, and  $I_{sh}$  is the shunt current flowing through the resistance  $R_{sh}$ . In a PV cell, the generated current is directly proportional to solar irradiation. The photocurrent generated by the solar cell is given by (2).

$$I_{ph} = G[I_{SC} + K_i(T_{op} - T_{ref})] \quad (2)$$

In (2),  $G$  represents solar irradiance in  $W/m^2$ ,  $I_{sc}$  is the short circuit current,  $K_i$  represents the temperature coefficient, and  $T_{op}$  is the operating temperature.  $T_{ref}$  is the reference temperature which is considered  $25^\circ C$ . At standard test conditions (STC), solar irradiance is considered  $1000 W/m^2$ . The (3) gives the diode current.

$$I_d = I_s \left[ e^{q \left( \frac{V_{PV} + I_{PV} R_s}{N_s n V_t C} \right)} - 1 \right] \quad (3)$$

In (3),  $I_s$  represents the diode reverse saturation current, and the elaborated expression for saturation current  $I_s$  is depicted in (4);  $V_{pv}$  is the output voltage of the PV cell,  $R_s$  is the series resistance which is considered as  $0.01\text{-ohm}$ ,  $N_s$  is the number of cells connected in series,  $v_t$  is the terminal voltage,  $C$  is the number of cells in the module and  $n$  is the ideality factor.

$$I_s = I_{rs} \left( \frac{T_{op}}{T_{ref}} \right)^3 e^{\left[ \left( \frac{1}{T_{op}} - \frac{1}{T_{ref}} \right) \left( \frac{E_g q}{K n} \right) \right]} \quad (4)$$

In (4),  $q$  represents the charge of an electron, which is equal to  $1.6 \times 10^{-19} C$   $E_g$  denotes band gap energy,  $K$  is the Boltzmann constant, and the value of  $K$  is  $1.38 \times 10^{-23} J/K$ . The variable  $I_{rs}$  represents diode reverse saturation current at STC, and the mathematical expression is given by (5).

$$I_{rs} = \frac{I_{sc}}{\left[ e^{\left( \frac{q V_{oc}}{K C T_{op} n} \right)} - 1 \right]} \quad (5)$$

The reverse saturation current  $I_{rs}$  depends on the short circuit current  $I_{sc}$ . The mathematical expression for shunt current ( $I_{sh}$ ) is given by (6).

$$I_{sh} = \left[ \frac{V_{PV} + (I_{PV} R_s)}{R_{sh}} \right] \quad (6)$$

In (6),  $R_{sh}$  represents the shunt resistance value, as shown in Figure 1. By combining (1)-(6), a MATLAB/Simulink model is developed, and obtained the PV panel characteristics for  $250 W$  polycrystalline solar panel. The Simulink model of the  $250 W$  solar panel is illustrated in Figure 2.

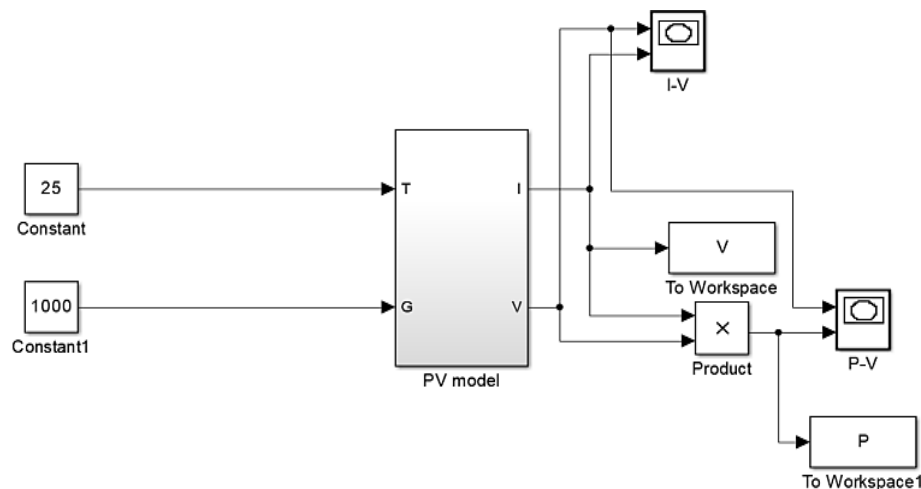


Figure 2. MATLAB/Simulink model of 250 W solar panel

As mentioned earlier, six modeling equations are made into a subsystem, shown in Figure 2. The characteristics were plotted to understand the operating features of a given solar panel. The electrical characteristics, such as I-V and P-V curves, are illustrated in Figures 3 and 4, respectively.

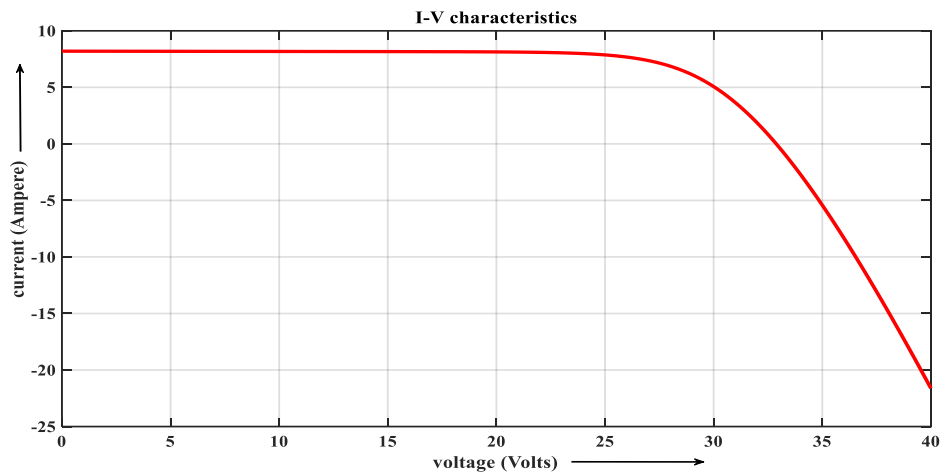


Figure 3. I-V characteristics of PV panel

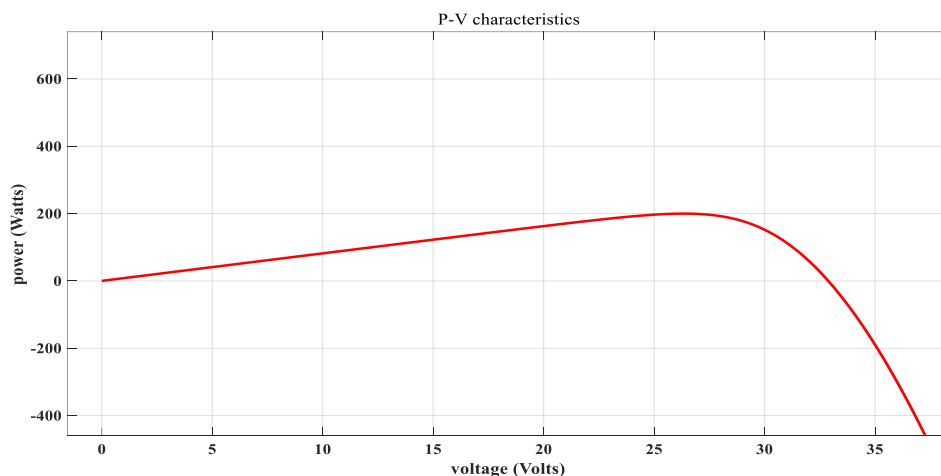


Figure 4. P-V characteristics of PV panel

Found that the I-V curve is non-linear. The I-V curve obtains the solar panel's open circuit voltage ( $V_{oc}$ ) and short circuit current ( $I_{sc}$ ). Here the  $V_{oc}$  is 39 V, and the  $I_{sc}$  is 8.21 A. The maximum power can be estimated using the P-V curve illustrated in Figure 4. Real-time testing of 250 W polycrystalline solar panels is carried out. The specification of a 250 W solar panel is given in Table 1.

The real-time testing is carried out using a 250 W, Polycrystalline solar panel and obtains the following results. The P-V curve of 250 W, polycrystalline solar panel is shown in Figure 5 at different time duration. The I-V curve of 250 W, polycrystalline solar panel is shown in Figure 6 at different time.

The effect of temperature and solar irradiance are studied in this research. Generally, solar irradiance changes from time to time during the day. As the irradiance is high, the output voltage of a PV panel increases; this leads to an increase in the output power of the PV panel. The variation of irradiance to the output voltage of the PV panel is shown in Figure 7.

In Figure 7, irradiance changed from  $500 \text{ W/m}^2$  to  $1200 \text{ W/m}^2$ . The maximum voltage across the PV panel is when the irradiance is  $1200 \text{ W/m}^2$ , and the voltage across the panel is less when the irradiance changes to  $500 \text{ W/m}^2$ . Temperature is another factor directly impacting the performance of PV panels. In this study, the temperature of the PV panel varied from  $25^\circ\text{C}$  to  $50^\circ\text{C}$ . As the temperature of the PV panel increases, the voltage across the solar panel is reduced, as shown in Figure 8. The PV panel is to be operated

at the optimum temperature specified in the nameplate rating to achieve maximum power output. Moreover, operating the PV panel during maximum irradiance conditions is desirable. Figures 7 and 8 indicate the study of the effect of variation of temperature and irradiance in the PV panel.

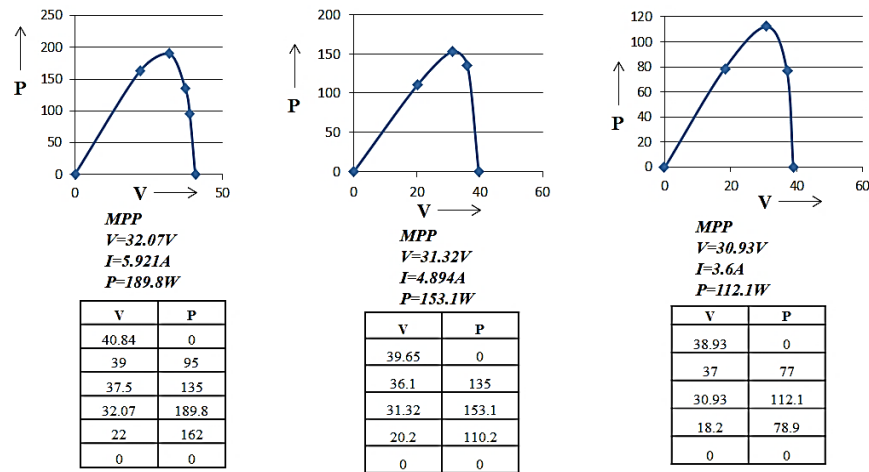


Figure 5. P-V characteristics of 250 W solar panel in real time testing

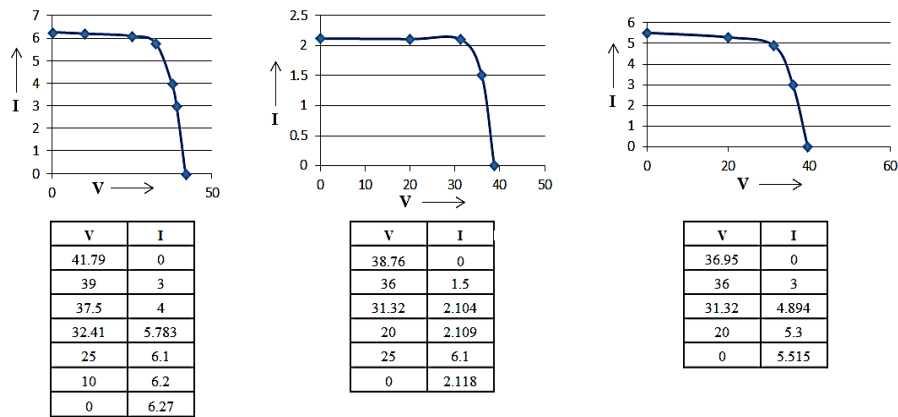


Figure 6. I-V characteristics of 250 W solar panel in real time testing

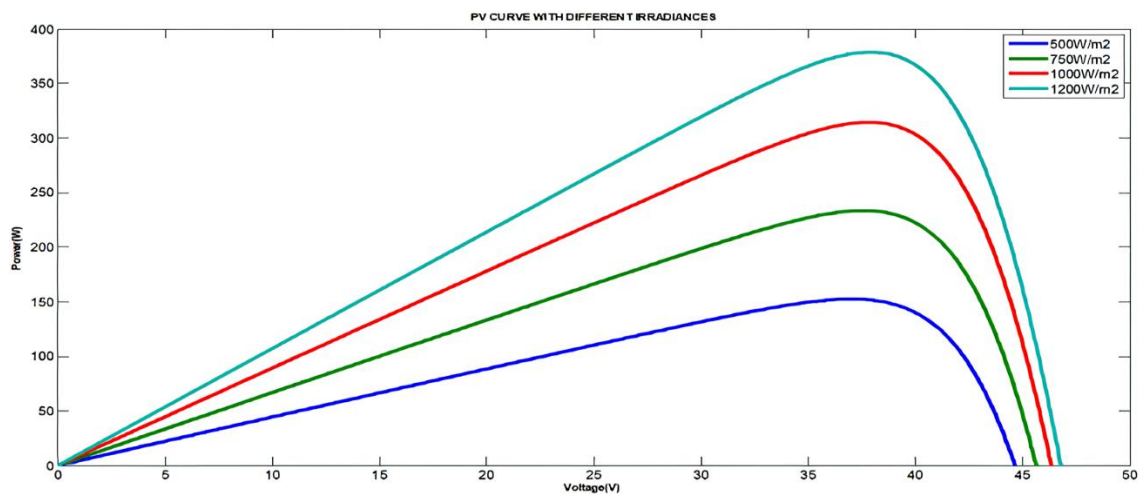


Figure 7. Effect of irradiance on PV panel output

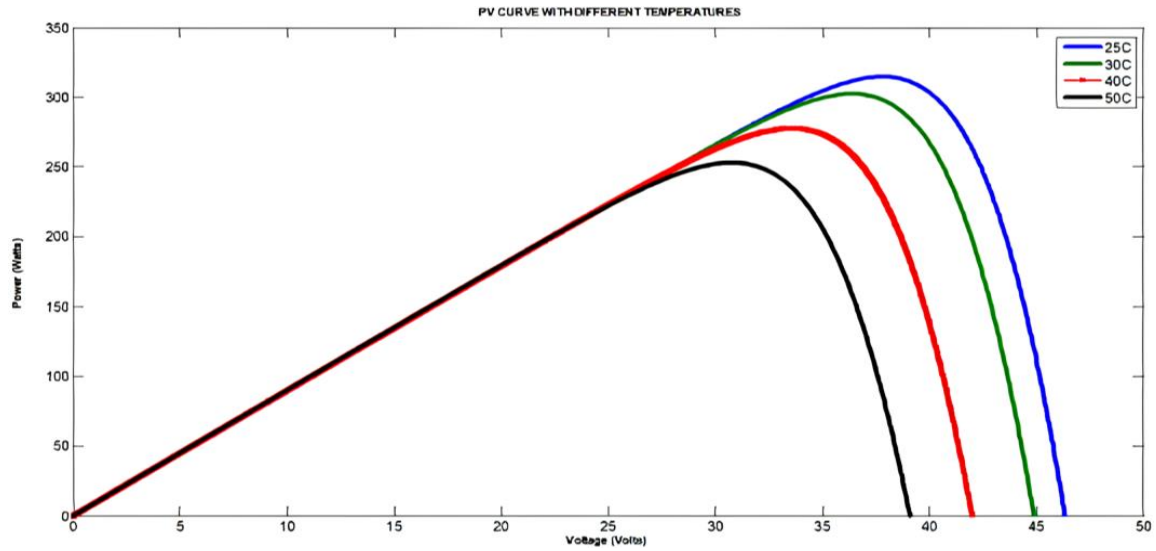


Figure 8. Effect of temperature on PV panel output

Table 1. Specification of solar panel

System specification	Rating
Power rating	250 W
Open circuit voltage, $V_{oc}$	39 V
Short circuit current, $I_{sc}$	8.21 A
Operating voltage, $V_o$	24 V
Series resistance, $R_s$	0.221 $\Omega$
Shunt resistance, $R_{sh}$	415.405 $\Omega$
Nominal temperature, $T_n$	25 °C or 298 K

## 2.2. Modes of operation of HEHG converter

HEHG converter consists of a high-side MOSFET switch, a coupled inductor ( $N_1$  and  $N_2$ ), and two switched capacitors ( $C_2$  and  $C_3$ ) shown in Figure 9. Switched capacitors are connected through power diodes  $D_2$  and  $D_3$ , respectively. A DC link capacitor is added to maintain constant voltage from the input supply and to obtain the ripple-free output capacitor;  $C_0$  is placed across the load. A modified ICA with the frequent sweeping of duty ratio is added as feed-forward control [8]. Maximum power point tracking (MPPT) control is connected to the gate of n channel power MOSFET through a gate driver circuit. A 250 W polycrystalline PV panel is the source, and the DC motor coupled with a centrifugal pump is considered the load [9].

In the HEHG converter, diode  $D_1$  and capacitor  $C_1$  recycle leakage inductance energy from the coupled inductor  $N_1$  and reduce voltage stress across the switch, thereby minimizing the switching losses. The switched capacitors of the HEHG converter maintain high voltage gain compared to the conventional DC-DC converter [10]. The function of each segment is clearly mentioned in Figure 9. The converter can be driven in continuous conduction mode, discontinuous conduction mode, and boundary conduction mode [11], [12]. Since the HEHG is selected for solar water pumping application, continuous conduction mode is selected as the operating mode. The continuous conduction mode is segmented into five segments. Also, the following assumptions are made for understanding the operation of the HEHG converter:

- All active and passive components used in the converter are ideal.
- Parasitic capacitance of MOSFET switch is neglected.
- Voltage drop across capacitors are considered to be constant.
- Equivalent Series Resistor (ESR) of a capacitor is neglected.
- Parasitic resistance of the coupled inductor is not considered.

The continuous conduction mode (CCM) of the HEHG converter is illustrated in Figure 10. The HEHG converter is driven in CCM [3]. CCM is segmented into five sub-intervals, as shown in Figure 10. Among five subintervals, two sub-intervals (1 and 2) are treated as ON intervals, and the remaining three (3, 4, and 5) are considered as OFF intervals. It is observed that sub-intervals 1, 3, and 4 occur in a short duration of time, whereas sub-intervals 2 and 3 take place over an extensive duration of time.

The sub-interval one starts at  $t_0$  and terminates at  $t_1$ . The MOSFET switch is on during this period. Magnetizing inductor  $L_m$  continuously releases energy to the switched capacitors  $C_2$  and  $C_3$ . The term  $L_{k1}$

represents stored energy from the DC source  $V_{in}$ . Energy stored in  $C_0$  is continuously discharged to the load. This sub-interval ends when the increasing value of  $I_{LK1}$  equals the decreasing value of  $I_{LM}$  at  $t = t_1$ . The input voltage  $V_{in}$  is serially connected to condensers  $C_1$ ,  $C_2$ , and  $C_3$ . Also, the input voltage is connected to the second terminals of coupled inductor  $N_2$  serially.  $L_{k2}$  discharges energy stored in output capacitor  $C_0$  and load  $R$ . In the meantime, magnetizing inductor  $L_m$  also acquires energy from the Input voltage  $V_{in}$ . Sub-interval 2 ends when the MOSFET switch  $S$  is turned OFF at  $t = t_2$ . Sub-interval 2 ends when the MOSFET switch  $S$  is turned off at  $t=t_2$ .

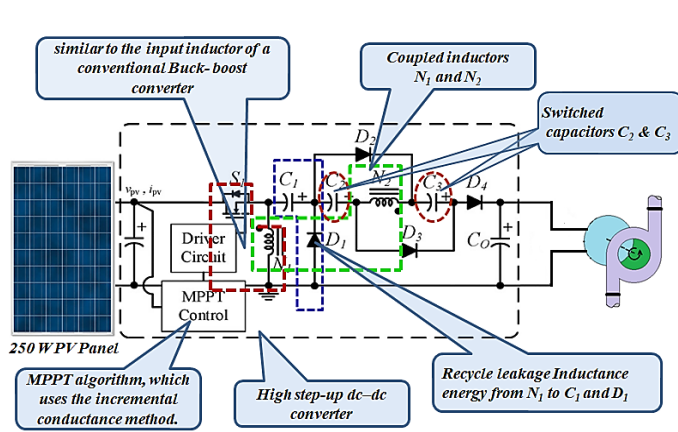


Figure 9. Circuit diagram of HEHG converter

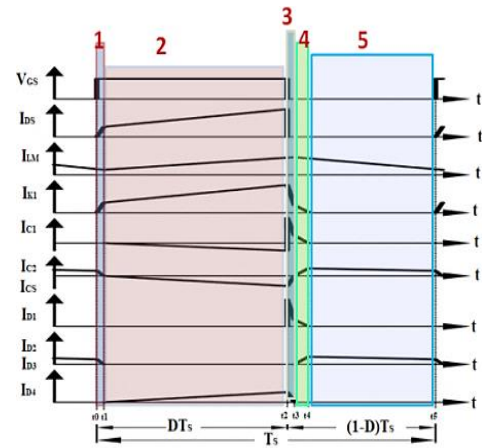


Figure 10. Modes of operation

The circuit behavior during sub-interval three is shown in Figure 10. In this sub-interval energy stored in  $L_{k1}$  is instantly flows through diode  $D_1$  to charge capacitor  $C_1$ . At the same time, energy is discharged to magnetizing inductor  $L_m$  through coupled inductor  $N_2$ . The sub-interval three ends when decreasing in  $I_{LK1}$  equals increasing  $I_{LM}$  at  $t$  equals  $t_3$ . The time duration of sub-interval 3 is too short. In the sub interval 4,  $L_{k1}$  constantly to release energy to charge capacitor  $C_1$  through the power diode  $D_1$ . Magnetizing inductor  $L_m$  transfers energy through the coupled inductor  $T_1$  to the switched capacitors  $C_2$  and  $C_3$ . Energy stored in the output capacitor  $C_0$  is constantly discharged to load  $R$ . Sub-interval 4 concludes when the decreasing  $I_{LK1}$  reaches zero and time  $t$  approaches  $t_4$ . The value of  $V_{LM}$  is equal to the negative value of  $V_{CM}$ . Sub-interval 5 occurs when the MOSFET switch is in OFF condition. Sub-interval 5 concludes when the MOSFET is turned on at the start of the next switching period.

### 3. DESIGN OF HEHG CONVERTER

The implementation procedure of the HEHG is carried out using the following steps: checking the input and output parameters, estimating converter parameters and values of magnetics, calculating switched capacitors, and estimating the leakage inductance values [13]. The system parameters are summarized in Table 2.

Table 2. System parameters	
Parameters of solar panel	Rating
PV module power rating	250 W
Available input voltage	30 V
Output voltage of converter	400 V
Switching frequency	50 kHz

The duty ratio is an essential parameter of the HEHG converter. To set the duty ratio of the HEHG converter turns ratio of coupled inductor is to be decided. The voltage gain of the HEHG converter is specified in (7).

$$\frac{V_0}{V_{in}} = \frac{nD+n+1}{1-D} \quad (7)$$



The turn ratio is selected in the range of 2 to 6. Initially, the select turns ratio is equal to 2, putting the value of available input voltage and output voltage of the converter in (15), the value of the duty ratio becomes 63.66%. If the converter switch is operated at 63.66%, high forward conduction losses take place in the circuit, and this results in reducing the overall efficiency. The select turns ratio of coupled inductor is four, and obtained value of the duty ratio is 40.656%. Whenever the turns ratio is equal to 6, the duty ratio becomes 32.74% which results in less value of magnetizing inductance but  $I_{peak}$  over MOSFET. Therefore, the optimal selection of turns ratio is four, and operate the converter at a duty ratio of 40.656%. The highest gain provided by the HEHG converter is 13.33. To estimate the magnetizing inductance, the magnetization time constant  $\tau_{LB}$  is to be determined first.

$$\tau_{LB} = \frac{D(D-1)^2}{2(2n+1)(nD+n+1)} \quad (8)$$

The value of magnetizing inductance by substituting other parameters in (16) is  $2.16 \times 10^{-3}$ . Once the value of magnetizing inductance is obtained, calculate the value of magnetization inductance ( $L_m$ ) using (9).

$$L_m = \tau_{LB} R T_s \quad (9)$$

$T_s$  is the pulse period, the reciprocal of the switching frequency ( $f_s$ ), and the calculated value of magnetizing inductance ( $L_m$ ) is 27.6  $\mu$ H. The value of  $L_m$  is treated as the primary value of Inductance ( $L_1$ ) of coupled Inductor. Likewise, the secondary inductance ( $L_2$ ) is calculated using (10).

$$\frac{N_1}{N_2} = \left( \frac{L_1}{L_2} \right)^{\frac{1}{2}} \quad (10)$$

The value of the secondary inductance of the coupled inductor is 442  $\mu$ H.  $L_{K1}$  and  $L_{K2}$  are calculated using 1% of  $L_1$  and  $L_2$ , respectively. Therefore, the estimated values of  $L_{K1}$  are 0.2765  $\mu$ H and  $L_{K2}$  4.42  $\mu$ H, respectively. The presence of a resistive component in the coupled inductor is calculated using (11).

$$R_{base} = \frac{(V_{peak} \times D)^2}{P_n} \quad (11)$$

The obtained value of  $R_{base}$  is 0.8483  $\Omega$ .  $P_n$  is considered the power rating of the converter. In the same way, the per unit value of resistance ( $R_{pu}$ ) is determined using (12).

$$R_{pu} = \frac{R}{R_{base}} \quad (12)$$

$L_{base}$  is obtained using (21). Also,  $L_{base}$  depends on the switching frequency of the MOSFET switch ( $f_s$ ) and  $R_{base}$ .

$$L_{base} = \frac{R_{base}}{2\pi f_s} \quad (13)$$

Substituting the values of  $R_{base}$  and  $f_s$  in (13), and designed value of  $L_{base}$  is 2.701  $\mu$ H. Per unit value of inductance is obtained using (14).

$$L_{pu} = \frac{L}{L_{base}} \quad (14)$$

The mean value of the resistive component ( $R_m$ ) is calculated using (15). The  $R_m$  depends on the value of inductive reactance and the base value of resistance ( $R_{base}$ ). The estimated value of  $R_m$  is 10.23 ohm.

$$R_m = \frac{X_L}{R_{base}} \quad (15)$$

The values of capacitors are designed using (16), (17), and (18). The input capacitor ( $C_1$ ) is calculated as (16).

$$C_1 = \frac{I_0 \times T_s}{\Delta V_{C1}} \quad (16)$$

Here  $I_0$  denotes the current flowing through the load, and  $\Delta V_{C1}$  represents ripple voltage which is assumed as 20% of voltage across the capacitor  $V_{C1}$ . The obtained value of  $C_1$  is 16.98  $\mu$ F.  $C_2$  and  $C_3$  have switched



capacitors in the circuit diagram, which help maintain high gain for the HEHG converter. The design calculation of switched capacitor is calculated as (17).

$$C_2 = C_3 = \frac{I_0 T_s}{\Delta V_{C2}} \quad (17)$$

The designed value of switched capacitors is 4.425  $\mu\text{F}$ . To maintain the output voltage without fluctuating, output capacitor  $C_0$  is used.

$$C_0 = \frac{I_0 \times D \times T_s}{\Delta V_0} \quad (18)$$

Using (18), the obtained value of  $C_0$  is 0.423  $\mu\text{F}$ . The parameters related to HEHG and the value of magnetics are designed and tabulated in Table 3. The calculated values and practical values of capacitors are shown in the Table 4. The detailed design procedures of the coupled inductor and switched capacitors are explained in detail with certain assumptions. The designed values are used in MATLAB simulation of the HEHG DC-DC converter.

Table 3. Design parameters of HEHG converter and value of magnetics

Parameters	Calculated values	Practical values
Voltage gain	13.33	14
Turns ratio	2,4 and 6	4
Duty ratio	63.66%, 40.656%, and 32.74%	40.656%
Magnetization time constant	2.16 ms	2.16 ms
Magnetization inductance ( $L_1$ )	27.6 $\mu\text{H}$	30 $\mu\text{H}$
Magnetization inductance ( $L_2$ )	442 $\mu\text{H}$	470 $\mu\text{H}$

Table 4. Designed values of capacitors

Parameters	Calculated values	Practical values
$C_1$	16.98 $\mu\text{F}$	22 $\mu\text{F}$
$C_2$	4.42 $\mu\text{F}$	4.7 $\mu\text{F}$
$C_3$	4.42 $\mu\text{F}$	4.7 $\mu\text{F}$
$C_0$	0.42 $\mu\text{F}$	0.47 $\mu\text{F}$

## 4. RESULTS AND DISCUSSION

HEHG converter is designed to meet the system requirements. The simulation and hardware are implemented using the designed value. Both the simulation and hardware results are explained in this chapter. Furthermore, the HEHG converter is compared with the conventional DC-DC boost converter to perform the validation.

### 4.1. Simulation of HEHG converter

The simulation of the HEHG converter is carried out using the MATLAB/Simulink platform. Overall Simulink model is segmented into PV panel modeling, converter modeling, and modeling of load. A modified ICA D-sweep technique is added to the HEHG to improve tracking accuracy. The Simulink model is developed using the designed values shown in Tables 3 and 4. Feed-forward control is adopted in this system in the form of the ICA D-sweep MPPT technique. The Simulink model of the HEHG converter is illustrated in Figure 11.

The model of HEHG converter is simulated for 0.2 s, and the electrical parameters such as voltage, current, and power are obtained at the input and output of the HEHG converter. The efficiency of HEHG is also determined. The input variables, such as voltage, current, and available power, are shown in Figure 12. The available input voltage from the PV panel is 35.92 V. Therefore HEHG converter is operated at 35.92 V. Input voltage becomes stable at 0.1 s. It is observed that input power and current become stable at 0.08 s. It is observed that the input current of the HEHG converter is 6.034 A. Also, the available input power from the SPV panel is 216.7 W. Availability of input power depends on solar irradiance and the operating temperature of the PV panel. The switching stress on the MOSFET of the HEHG converter is also mentioned in Figure 12. The average switching stress on the MOSFET switch of the HEHG converter is 28.5 V which can be mitigated using a regenerative snubber circuit.

The model of HEHG converter is simulated for 0.2 s, and the electrical parameters such as voltage, current, and power are obtained at the input and output of the HEHG converter. The efficiency of HEHG is

also determined. The input variables, such as voltage, current, and available power, are shown in Figure 12. The available input voltage from the PV panel is 35.92 V. Therefore HEHG converter is operated at 35.92 V. Input voltage becomes stable at 0.1 s. It is observed that input power and current become stable at 0.08 s. It is observed that the input current of the HEHG converter is 6.034 A. Also, the available input power from the SPV panel is 216.7 W. Availability of input power depends on solar irradiance and the operating temperature of the PV panel. The switching stress on the MOSFET of the HEHG converter is also mentioned in Figure 12. The average switching stress on the MOSFET switch of the HEHG converter is 28.5 V which can be mitigated using a regenerative snubber circuit.

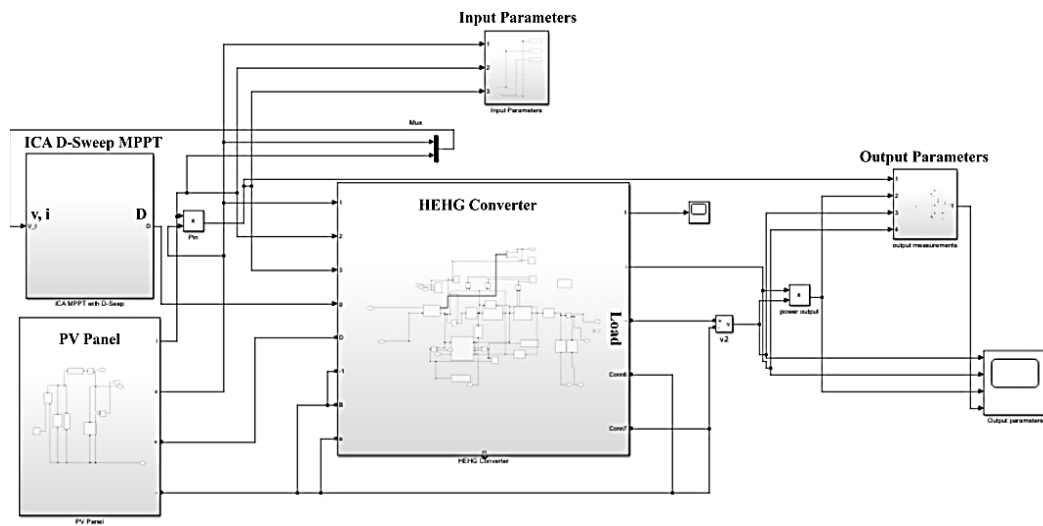


Figure 11. Simulink model of HEHG DC-DC converter

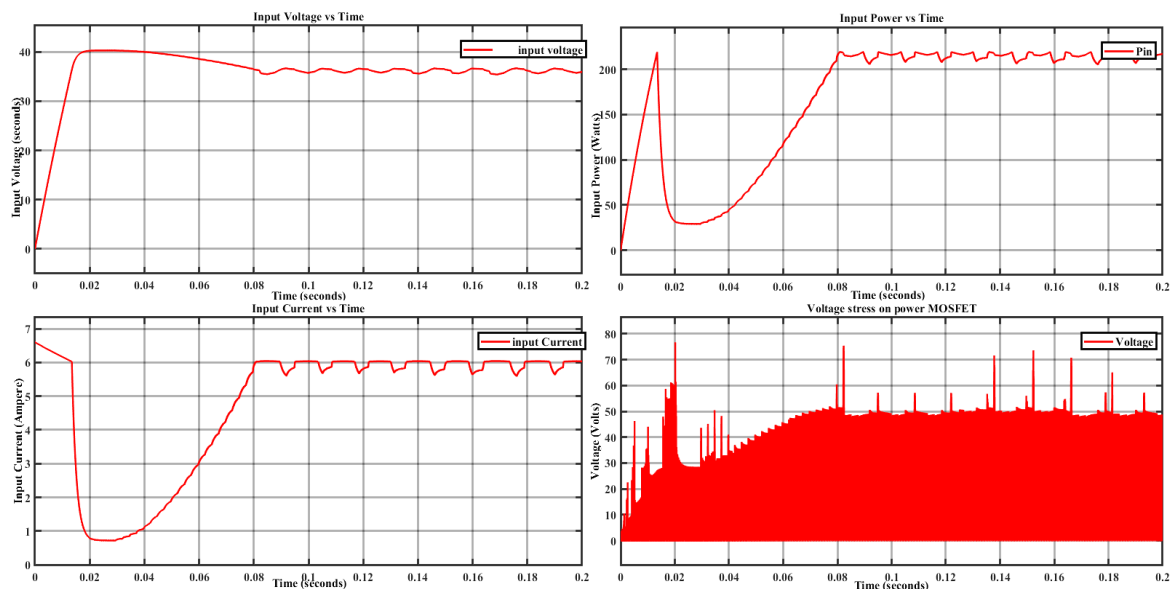


Figure 12. Input parameters of HEHG converter

The output voltage and current depend upon the load connected to the HEHG converter. The output voltage sensed through the load is 418.5 V, and the current through the load is 0.49 A. The obtained output power value is 208.10 W, as indicated in Figure 13. The net efficiency of the HEHG converter is calculated by taking the output power to input power ratio. The average input power obtained at the HEHG converter is 216.7 W, and the output power across the load is 208.10 W. Found that output parameters such as current, voltage, and power have become stable at 0.2 s. The efficiency of the HEHG converter is calculated using (19).

$$\text{Efficiency}, \eta = \frac{\text{output power}}{\text{input power}} \times 100 \quad (19)$$

Using (27), the obtained value of the efficiency is 96.01%. The efficiency of the HEHG converter is indicated in Figure 13. The overall voltage gain of the HEHG converter is 11.65. On the other side, it shows high efficiency without compromising its overall gain. The efficiency of the HEHG converter is obtained maximum when the simulation time reaches 0.1 s.

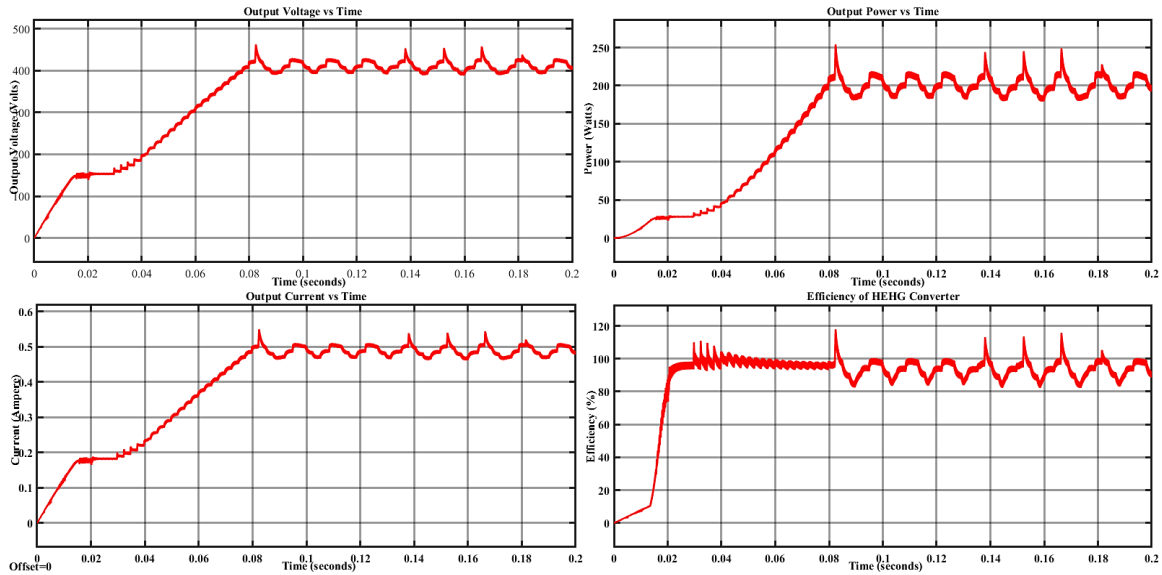


Figure 13. Output parameters of HEHG converter

#### 4.2. Hardware implementation of HEHG converter

Hardware prototype includes the development of a power circuit and control circuit [14]. Hardware components are selected using the simulation carried out using MATLAB/Simulink. Current through each component and voltage across the components is determined first. Checked the availability of components in the market and studied the datasheet. Current through the passive and active components, the voltage across the active and passive components is specified in Table 5.

Table 5. Hardware components of HEHG converter

Name of the component	Specification	Voltage across	Current through
Power MOSFET	IRFP250N	120 V	40 A peak spike
Power diode D <sub>1</sub>	MUR 1560	100 V	20 A peak spike
Power diode D <sub>2</sub>	MUR 1560	400 V	2 A peak spike
Power diode D <sub>3</sub>	MUR 1560	100 V	2 A peak spike
Power diode D <sub>4</sub>	MUR 1560	300 V	10 A
Capacitor C <sub>1</sub>	22 $\mu$ F/250 V	92 V	12 A
Switched capacitor C <sub>2</sub>	4.7 $\mu$ F/250 V	100.5 V	8.4 A
Switched capacitor C <sub>2</sub>	4.7 $\mu$ F/250 V	100.5 V	8.4 A
Capacitor C <sub>0</sub>	0.47 $\mu$ F/1200 V	418.5 V	6 A
Coupled inductor (L <sub>1</sub> and L <sub>2</sub> )	30 $\mu$ H and 470 $\mu$ H	78.05 V, 27.82 V	12.4 A and 18.3 A

The core of the coupled inductor is made up of E55 type. The winding of the coupled inductor is made up of enameled copper with a thickness of 22 standard wire gauge (SWG). Mylar sheet is provided proper isolation between the primary and secondary sides of the coupled inductor. The main function of a mylar sheet is to prevent the arcing of the primary and secondary sides of the coupled inductor. The quality factor (Q) of L<sub>1</sub> and L<sub>2</sub> are 72.62 and 68.52, respectively. The components mentioned in Table 5 are assembled using glass epoxy printed circuit board. ICA MPPT has been developed using AVR Atmega 38 microcontroller. The block diagram shown in Figure 14 helps to understand the hardware implementation [15], [16] of the HEHG converter.

The overall circuit is divided into a power and control circuit. The power circuit consists of a solar panel supplied to the load through a HEHG converter. A pulse width modulation (PWM) is generated in the form of MPPT using a control assisting circuit [17]–[22]. A 7805-voltage regulator integrated circuit (IC) is supplied 5 V to AVR Atmega 32, and the output pin of AVR Atmega 32 is fed to gate driver IC and designed current and voltage sensor circuits to implement MPPT. Here, an optocoupler IC, namely TLP 250, is selected for the gate driving and isolating power and control circuits, which is operated 15 V DC power supply shown in Figure 14. The output of TLP 250 and the load is shown in Figures 15(a) and 15(b).

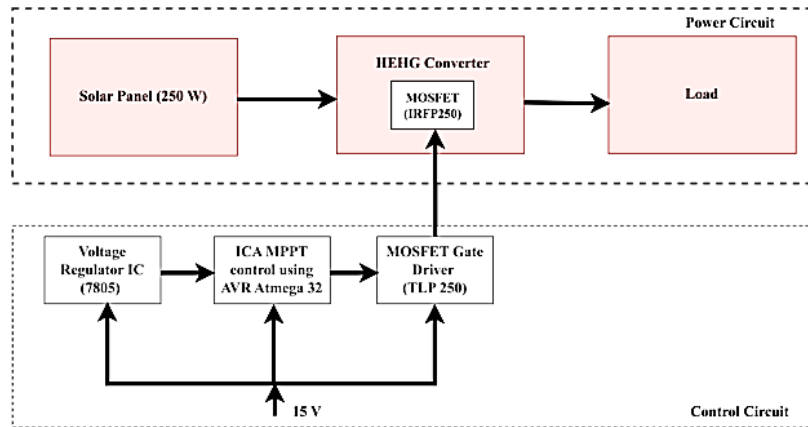


Figure 14. Hardware implementation of HEHG converter

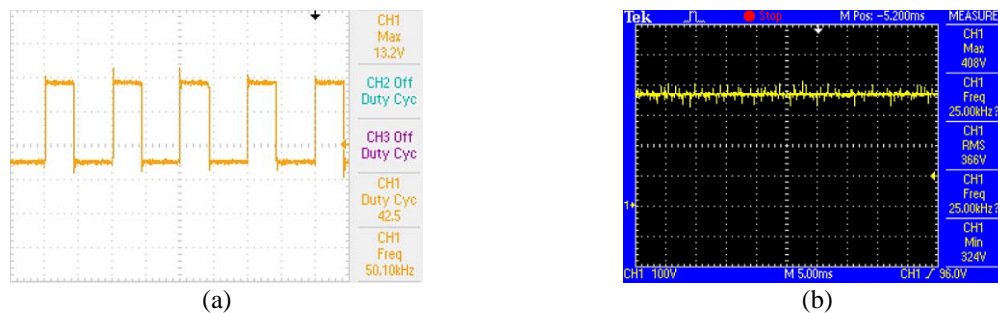


Figure 15. Output voltage across (a) TLP 250 gate driver IC and (b) the load

A prototype of the HEHG converter is implemented and conducted in the real-time test. Initially, the PWM corresponding to D-Sweep MPPT is developed using an AVR Atmega 32 microcontroller which is the control part of the system. A suitable gate driver, TLP 250, is added to ensure the isolation of power and control circuits [23]. The second stage implements the power circuit and integrates both power and control circuits. The overall setup of the hardware prototype is shown in Figure 16. It depicts how the components are assembled. The power part and control parts are illustrated in this section.



Figure 16. Hardware setup of HEHG DC-DC converter

The real-time testing of the HEHG converter is conducted. The following performance parameters were obtained. Table 6 provides the details of the hardware result. The fundamental components are assembled on a board. Initially, the components were rigged up on a breadboard, and conducted the testing. The following parameters were obtained. Table 6 provides the details of the hardware result.

Table 6. Hardware results of HEHG converter

Parameters	Rating
Input voltage	32.5 V
Input current	7.2 A
Output voltage	408 V
Current through the load	0.54 A
Voltage stress on the switch	28.5 V

The available input power from the solar panel is 230.4 W, and the output power obtained at the load is 220.32 W. Therefore, overall power conversion efficiency of the HEHG converter is 95.62%. Another critical observation is there is a tallying of simulation and hardware results. To validate the work, HEHG hardware result is compared with conventional DC-DC boost converter [24]–[26]. The hardware set up (power circuit) of conventional boost converter is shown in Figures 17 and 18.

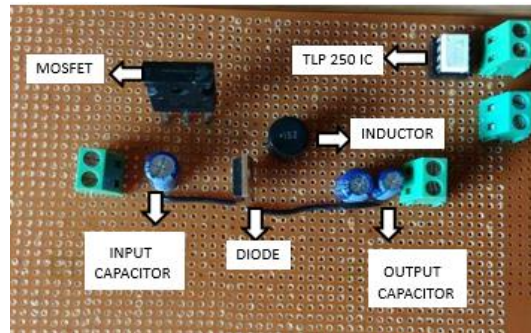


Figure 17 Prototype of DC-DC boost converter

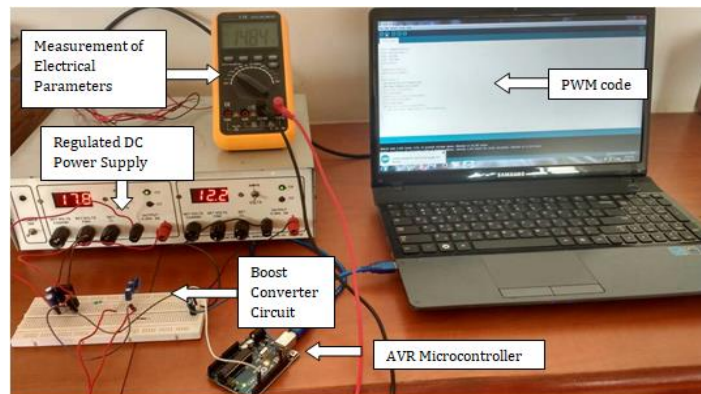


Figure 18. Hardware set up DC-DC boost converter

The PWM corresponding to MPPT is implemented using an AVR microcontroller. The comprehensive set of the conventional DC-DC boost converter is shown in Figure 18. An optocoupler IC, TLP 250, helps to maintain the isolation of power and control circuits. The input voltage of 30 V is used. The inductance of 0.2 mH, output capacitance of 0.2 mF, and power MOSFET-IRFP250N and power diode-MUR1560 is used for the hardware implementation.

The comparison of the HEHG converter with the conventional boost converter is given in Table 7. The parameters include voltage gain, efficiency, voltage stress on the switch, and the number of switches used. It is observed that a solar photovoltaic system operating in the range of 30 V to 40 V will be boosted the voltage level of 400 V to meet the load requirements, and both converters can be used. However, as the voltage gain increases, there is a reduction in the efficiency of the boost converter due to high voltage stress across the switch. Also, the rate of efficiency of the HEHG converter is superior to that traditional boost converter. However, the number of passive components used in HEHG is higher than in the conventional boost converter. Though the count of passive components is more, there is no considerable difference in the overall hardware implementation cost.

Table 7. Comparison of HEHG converter with conventional boost converter

Parameters	Conventional boost converter	HEHG converter
Voltage gain	$1$	$nD + n + 1$
Efficiency	$\frac{1-D}{81.25\%}$	$\frac{1-D}{95.62\%}$
Voltage stress	58.76 V	28.5 V
Number of power switches	1	1
Number of capacitors used	2	5

## 5. CONCLUSION

A high efficient power electronic interface is essential for the solar photovoltaic system to overcome the challenges such as poor conversion efficiency and shading effect. The unsuitability of conventional boost converters can be overcome by using high efficient high gain converter, especially for high voltage high gain applications. The presence of switched capacitors and coupled inductors help to reach target of high voltage gain and reduced switching losses. MATLAB/Simulink model is developed as per the design. The HEHG converter is designed and simulated for 0.2 s, and the efficiency of the HEHG converter is 96.01% with a voltage gain of 11.65. A hardware prototype of the HEHG converter is implemented using the same design values. Performance parameters such as efficiency and voltage gain are measured during real-time testing. The obtained efficiency of the HEHG converter during real-time testing is 95.62%, with a voltage gain of 12.55. Also, the performance of the HEHG converter with a conventional DC-DC boost converter is compared in accordance to the value of gain, efficiency, number of passive components used, and voltage stress on the MOSFET switch. It is concluded that the HEHG converter shows superior performance to the traditional boost converter. Also, the performance of HEHG converter can be still improved by adding a regenerative snubber circuit in the HEHG converter.

## REFERENCES




- [1] P. Górecki and K. Górecki, "Methods of fast analysis of DC–DC converters—a review," *Electronics*, vol. 10, no. 23, p. 2920, Nov. 2021, doi: 10.3390/electronics10232920.
- [2] S. Ranganathan and A. N. D. Mohan, "Formulation and analysis of single switch high gain hybrid DC to DC converter for high power applications," *Electronics*, vol. 10, no. 19, p. 2445, Oct. 2021, doi: 10.3390/electronics10192445.
- [3] S. Saravanan and N. R. Babu, "A modified high step-up non-isolated DC-DC converter for PV application," *Journal of Applied Research and Technology*, vol. 15, no. 3, pp. 242–249, Jun. 2017, doi: 10.1016/j.jart.2016.12.008.
- [4] J. Ahmad *et al.*, "A new high-gain DC-DC converter with continuous input current for DC microgrid applications," *Energies*, vol. 14, no. 9, p. 2629, May 2021, doi: 10.3390/en14092629.
- [5] Y. T. R. Palleswari and V. Rajendran, "A novel hybrid high gain DC-DC converter for renewable energy applications," *International Journal of Renewable Energy Research*, vol. 12, no. 1, pp. 88–96, 2022, doi: 10.20508/ijrer.v12i1.12554.g8376.
- [6] A. Al-Ateeq and A. J. Alateeq, "Soft-charging effects on a high gain DC-to-DC step-up converter with PSC voltage multipliers," *Engineering, Technology & Applied Science Research*, vol. 10, no. 5, pp. 6323–6329, Oct. 2020, doi: 10.48084/etasr.3773.
- [7] S. Pereira, E. F. M. Abreu, M. Iakunin, A. Cavaco, R. Salgado, and P. Canhoto, "Method for solar resource assessment using numerical weather prediction and artificial neural network models based on typical meteorological data: application to the south of Portugal," *Solar Energy*, vol. 236, pp. 225–238, Apr. 2022, doi: 10.1016/j.solener.2022.03.003.
- [8] K. S. Tey and S. Mekhilef, "Modified incremental conductance MPPT algorithm to mitigate inaccurate responses under fast-changing solar irradiation level," *Solar Energy*, vol. 101, pp. 333–342, Mar. 2014, doi: 10.1016/j.solener.2014.01.003.
- [9] A. Hilali, Y. Mardoude, A. Essahlaoui, A. Rahali, and N. El Ouanjli, "Migration to solar water pump system: environmental and economic benefits and their optimization using genetic algorithm Based MPPT," *Energy Reports*, vol. 8, pp. 10144–10153, Nov. 2022, doi: 10.1016/j.egyr.2022.08.017.
- [10] L. Senapati, M. M. Garg, A. K. Panda, and R. K. Lenka, "Topology synthesis and control of integrated three-port converter for renewable energy system," *Computers and Electrical Engineering*, vol. 101, p. 107996, Jul. 2022, doi: 10.1016/j.compeleceng.2022.107996.
- [11] B. P. L. Lau *et al.*, "A survey of data fusion in smart city applications," *Information Fusion*, vol. 52, pp. 357–374, Dec. 2019, doi: 10.1016/j.inffus.2019.05.004.
- [12] S.-M. Chen, T.-J. Liang, and K.-R. Hu, "Design, analysis, and implementation of solar power optimizer for DC distribution system," *IEEE Transactions on Power Electronics*, vol. 28, no. 4, pp. 1764–1772, Apr. 2013, doi: 10.1109/TPEL.2012.2213270.






- [13] J. D. Navamani, A. Lavanya, D. Almakhlis, and M. J. Sathik, "A review on segregation of various high gain converter configurations for distributed energy sources," *Alexandria Engineering Journal*, vol. 61, no. 1, pp. 675–700, Jan. 2022, doi: 10.1016/j.aej.2021.06.026.
- [14] Y. Koç, Y. Birbir, and H. Bodur, "Non-isolated high step-up DC/DC converters – an overview," *Alexandria Engineering Journal*, vol. 61, no. 2, pp. 1091–1132, Feb. 2022, doi: 10.1016/j.aej.2021.06.071.
- [15] S. Farhani, E. M. Barhoumi, and F. Bacha, "Design and hardware investigation of a new configuration of an isolated DC-DC converter for fuel cell vehicle," *Ain Shams Engineering Journal*, vol. 12, no. 1, pp. 591–598, Mar. 2021, doi: 10.1016/j.asej.2020.07.014.
- [16] M. A. Husain, A. Tariq, S. Hameed, M. S. Bin Arif, and A. Jain, "Comparative assessment of maximum power point tracking procedures for photovoltaic systems," *Green Energy & Environment*, vol. 2, no. 1, pp. 5–17, Jan. 2017, doi: 10.1016/j.gee.2016.11.001.
- [17] S. Suraj, J. J. J., and S. Soman, "Analysis of dual phase dual stage boost converter for photovoltaic applications," *International Journal on Advanced Science, Engineering and Information Technology*, vol. 10, no. 3, pp. 920–928, Jun. 2020, doi: 10.18517/ijaseit.10.3.5346.
- [18] M. Killi and S. Samanta, "An adaptive voltage-sensor-based MPPT for photovoltaic systems with SEPIC converter including steady-state and drift analysis," *IEEE Transactions on Industrial Electronics*, vol. 62, no. 12, pp. 7609–7619, Dec. 2015, doi: 10.1109/TIE.2015.2458298.
- [19] C. B. N. Fapi, M. Kamta, and P. Wira, "A comprehensive analysis of MPPT algorithms to optimal power extraction of a PV panel," *Journal of Solar Energy Research*, vol. 4, no. 3, pp. 172–179, 2019.
- [20] P. Pandiyan *et al.*, "Implementation of different MPPT techniques in solar PV tree under partial shading conditions," *Sustainability*, vol. 13, no. 13, p. 7208, Jun. 2021, doi: 10.3390/su13137208.
- [21] H. A. Mohamed-Kazim, I. Abdel-Qader, and A. M. Harb, "Efficient maximum power point tracking based on reweighted zero-attracting variable stepsize for grid interfaced photovoltaic systems," *Computers and Electrical Engineering*, vol. 85, p. 106672, Jul. 2020, doi: 10.1016/j.compeleceng.2020.106672.
- [22] I. Hamdan, A. Maghraby, and O. Noureldeen, "Random search optimization algorithm based control of supercapacitor integrated with solar photovoltaic system under climate conditions," *International Journal of Renewable Energy Research*, vol. 12, no. 2, pp. 611–622, 2022, doi: 10.20508/ijrer.v12i2.12616.g8479.
- [23] N. A. Windarko, M. N. Habibi, B. Sumantri, E. Prasetyono, M. Z. Efendi, and Taufik, "A new MPPT algorithm for photovoltaic power generation under uniform and partial shading conditions," *Energies*, vol. 14, no. 2, p. 483, Jan. 2021, doi: 10.3390/en14020483.
- [24] V. K. P. K. and K. Manjunath, "Analysis, design and implementation for control of non-inverted zeta converter using incremental conductance MPPT algorithm for SPV applications," in *2017 International Conference on Inventive Systems and Control (ICISC)*, Jan. 2017, pp. 1–5, doi: 10.1109/ICISC.2017.8068662.
- [25] V. K. P. K. and J. J. J., "Comparative analysis of bio-inspired maximum power point tracking algorithms for solar photovoltaic applications," *International Journal of Intelligent Systems and Applications in Engineering*, vol. 11, no. 1, pp. 100–110, 2023.
- [26] V. K. P. K. and J. J. J., "Comparative analysis of conventional and artificial intelligence-based maximum power point tracking algorithms for solar photovoltaic applications," *International Journal of Computer Applications*, vol. 184, no. 42, pp. 39–48, Jan. 2023, doi: 10.5120/ijca2023922526.

## BIOGRAPHIES OF AUTHORS



**Vineeth Kumar Pothera Kariyat**    is currently working as an Assistant Professor in the Department of Electronics and Communication Engineering at Sri Venkateshwara College of Engineering, Bengaluru, India. He received B.Tech degree in Electrical and Electronics Engineering from Kannur University, Kerala in 2011. He received M.Tech. degree in Power and Energy from Amrita Vishwavidyapeetham University, Coimbatore, Tamil Nadu, India. His area of interest includes power electronics and renewable energy resources. To his credit prolifically published eight papers in international conferences and three reputed international journals. He can be contacted at email: vineethkumarpk@gmail.com.



**Jijesh Jisha Janardhanan**    is currently working as Professor and HoD in the Electronics and Communication Department at Sri Venkateshwara College of Engineering, Bangalore. He received the B.Tech. degree in Electronics and Communication Engineering from Kannur University in 2006, and earned M.Tech. degree in Electronics from Visvesvaraya Technological University, Belgaum, in 2010 and awarded Doctorate Degree in the field of Wireless Communication from Visvesvaraya Technological University, Belgaum, in 2018-2019. He has more than 53 publications in his credit in various prestigious journals. His area of interest includes wireless communication, VLSI, and renewable energy sources. He can be contacted at email: jijeshjj4u@gmail.com.